



SPATIAL DOMAIN MODELING OF MICROCELLULAR SYSTEMS OPERATING IN MULTIPATH NAKAGAMI ENVIRONMENTS

Asrar U. H. Shiekh¹ and Saad Muhammed. Al-Ahmadi²

1: Chair professor, Department of Electrical Engineering, KFUPM.
Box 5038, Dhahran 31261. E-mail: asrarhaq@kfupm.edu.sa

2: Graduate assistant, College of Technology at Dammam
Box. 7650, Dammam 31472, Saudi Arabia.

ABSTRACT

In conventional channel models, the AoA's at the BS, are assumed to be uniformly distributed. However, measurements in urban areas have shown non-uniform AoA distributions. In this paper, the spatial characterization of wideband urban mobile radio channels is investigated and the resulting temporal and spatial correlations at the BS receiver are computed. A geometrically based modeling is used to spatially characterize both typical and bad urban environments. The clustered scatterers are assumed to have bivariate Gaussian densities. The AoA pdf's are derived. The temporal and spatial correlations are computed for both environments and the effects of the channel parameters such as the MS scatterer's variance, the BS-MS distance and the mean angle of arrival on these correlations are investigated.

Keywords: Geometrical models, Typical urban and bad urban areas, AoA statistics, Nakagami fading, spatial correlations.

AoA's

MS BS

1. INTRODUCTION

The increasing demand for higher data rates and user capacity in cellular systems has motivated the use of smaller cells and antenna arrays. However, the performance analysis of receiving systems such as 2-D RAKE receivers requires the appropriate spatio-temporal characterization of urban areas where:(i) The propagation characteristics in microcells (usually urban) are found [Turkmani et al,1989, Chia et al, 1987] to result in Rician or Nakagami fading characteristics rather than Rayleigh fading, which is the case in conventional urban macro-cellular systems. (ii) Measurements in different urban areas have shown that the widely used assumption that the AoA (Angle of Arrival) distribution (at the BS receiver) is uniform over a small angular range is not valid [Salz and Winters, 1994]. The AoA's were found to have truncated Gaussian and Laplacian distributions [Adachi et al, 1986, Pederson et al, 2000]. (iii) The spatial correlations among the received signals at the array elements have a major effect on the spatial diversity gain. These correlations are determined by the AoA distribution, the interelement spacing and the mean angle of arrival. In [Lee, 1973], the AoA's were assumed to have a raised cosine distribution to derive the spatial correlations at the BS for both the broadside and end fire cases. In [Salz and Winters, 1994], the AoA's were assumed to be uniformly distributed over the angular range $[-\Delta, \Delta]$ and the spatial correlations were computed for different values of Δ .

2. SPATIO-TEMPORAL CHANNEL MODEL

The equivalent spatio-temporal impulse response of the channel between a mobile transmitting using a single antenna and an M -element antenna array receiver at the BS is given as [Pederson et al, 2000]

$$h(t, \tau, \theta) = \sum_{l=1}^L \tilde{a}(t) \delta(t - \tau_l) V(\theta_l) \tag{1}$$

where L denotes the number of the multipath components, τ_l and θ_l are the average delay and the mean AoA of the l th path. $\tilde{a}(t)$ is the complex path vector, $\tilde{a}(t) = [a_1(t), \dots, a_M(t)]$. Each of the paths $a(t)$ can be expressed as the sum of a large number of time indifferetiable paths (TIS's) as

$$a(t) = \sum_{k=1}^{N_s} a_{ik} \exp(j\omega_m t \cos \alpha_{ik} + \varphi_{ik}) \tag{2}$$

where N_s denotes the number of TIS's (including possibly a line-of-sight (LOS) component), which have amplitudes a_{ik} , phases φ_{ik} maximum Doppler frequency ω_m , and AoA's α_{ik} (relative to the mobile velocity vector). The array response vector of the antenna array elements, $V(\theta)$, is given as

$$V(\theta_l) = [1, \dots, \exp(j2\pi(M-1)\Delta \sin \theta_l)], \quad l = 1, \dots, L. \tag{3}$$

where $\Delta = 2\pi d/\lambda$, λ is the wavelength of the arriving signal.

3. TU (TYPICAL URBAN) CHANNELS

3.1. Channel Model and Scatterers Distributions

The appropriate geometrical channel model for TU environments is shown in Fig. 1 where a wide band elliptical model is utilized. The effective scatterers are assumed to lie around both the MS and the BS in circles of radii R_m and R_b respectively.

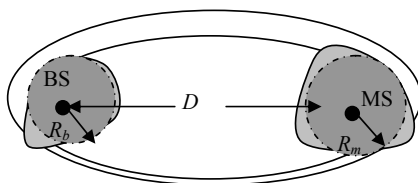


Figure 1: The geometrical model of TU channels.

The scatterers around the MS are assumed to have a bi-variate Gaussian distribution with a mean at the MS and variance σ_m so that the scatterer's pdf can be expressed in the polar coordinates (r_b, θ) as

$$p(r_b, \theta) = \frac{r_b}{2\pi\sigma_m^2} \exp\left[-\frac{(r_b^2 - 2r_b D \cos\theta + D^2)}{2\sigma_m^2}\right] \quad (4)$$

where r_b denotes the distance as measured from the BS to a scatterer 'S'. The variance, σ_m^2 , is an environment dependent parameter. However, assuming that the radius of significant scatterers around the MS ranges from 60 m to 150 m, [Lee, 1973, Fuhl et al, 1998], and assuming that the Gaussian pdf is significant over the range of 2.5 to 3 times the standard deviation, σ_m will range from 20-60 m. The scatterers around the BS are assumed to have a uniform distribution in the angular direction (θ) as

$$p_b(\theta) = \frac{1}{2\pi}, \quad -\pi < \theta < \pi \quad (5)$$

In the radial direction r_b , the scatterers are assumed to have Gaussian distributed with a mean at $(R_b/2)$ and variance σ_b as

$$p_b(r_b) = \frac{1}{\sqrt{2\pi}\sigma_b} \exp\left[-\frac{\left(r_b - \frac{R_b}{2}\right)^2}{2\sigma_b^2}\right] \quad (6)$$

The joint pdf, assuming independent marginal pdf's, can be expressed as [Papoulis, 1984]

$$p_b(r_b, \theta) = \frac{1}{2\pi\sqrt{2\pi}\sigma_b} \exp\left[-\frac{\left(r_b - \frac{R_b}{2}\right)^2}{2\sigma_b^2}\right] \quad (7)$$

3.2. AoA Statistics

The pdf of the AoA of the received wavefield in LOS TU micro-cells can be modeled using the concept of mixed distributions where the pdf can be expressed as the sum of two parameterized pdf's

$$p(\theta) = (1 - \sqrt{1 - m^{-1}}) \cdot p_d(\theta) + \sqrt{1 - m^{-1}} \cdot \delta(\theta - \theta_{LOS}) \quad , -\pi \leq \theta \leq \pi \quad , m \geq 1 \quad (8)$$

where m is the Nakagami fading parameter and θ_{LOS} is the AoA of the LOS component. The term $p_d(\theta)$ stands for the pdf of the diffused component, which can be expressed as

$$p_d(\theta) = p_1 \cdot p_m(\theta) + (1 - p_1) \cdot p_b(\theta) \quad (9)$$

where $p_m(\theta)$ denotes the AoA pdf of the portion of the diffused component that is due to the MS scatterers with a probability of p_1 and $p_b(\theta)$ denotes the AoA pdf of the portion due to the BS scatterers. In (9), the double scattering term was neglected due to the high attenuations in urban environments. The value of p_1 is an environment dependent parameter. However, in TU areas, the existence of densely distributed scatterers around the MS makes the probability of significant contribution of distant scatterers small (<0.2).

The AoA pdf's can be derived as

$$p(\theta) = \int_{r_{b1}(\theta)}^{r_{b2}(\theta)} p(r_b, \theta) dr_b \quad (10)$$

where $r_{b1}(\theta)$ and $r_{b2}(\theta)$ are the intersection points of the line $\theta = constant$ and the scatterers region. Carrying out integration with the appropriate limits results in the expression of $p_d(\theta)$ in (11) where the parameter R_{ns} denotes the radius of the circle of the "scatterers" that lie in the shadow region of the BS antenna array and hence are not expected to contribute to the received wavefield.

$$p_d(\theta) = \frac{p_1}{2\sqrt{2\pi}\sigma_m} \cdot D \cdot \cos\theta \cdot \exp\left[\frac{D^2(\cos^2\theta - 1)}{2\sigma_m^2}\right] \cdot \left[1 + \operatorname{erf}\left(\frac{D \cos\theta}{\sqrt{2}\sigma_m}\right)\right] + \frac{p_1}{2\pi} \cdot \exp\left(-\frac{D^2}{2\sigma_m^2}\right) + \frac{(1 - p_1)}{4\pi} \cdot \left[\operatorname{erf}\left(\frac{R_b}{2\sqrt{2}\sigma_b}\right) - \operatorname{erf}\left(\frac{R_{ns} - \left(\frac{R_b}{2}\right)}{\sqrt{2}\sigma_b}\right) \right] \quad , -\pi \leq \theta \leq \pi \quad (11)$$

The plot of the $p_d(\theta)$ in Fig. 2 shows that the angular spread in TU micro-cells areas (as seen at the BS) is concentrated around the BS-MS direct line over a range that increases as the scatterer's variance increases or the BS-MS distance decreases.

3.3. Doppler Power Spectrum and Temporal Correlations

The Doppler power spectrum (DPS) of the received wavefield can be expressed as [Stüber, 2001]

$$S(f) = (1 - \sqrt{1 - m^{-1}}) \cdot S_d(f) + \sqrt{1 - m^{-1}} \cdot \delta(f - f_o \cos \theta_{LOS}) \quad (12)$$

where $S_d(f)$ denotes the DPS of the diffused component and f_o is the frequency of the LOS component. The term $S_d(f)$ is given as in (13) [Jakes, 1974] where p is the average power that would be received by an isotropic antenna, f_m is the maximum Doppler frequency and $G(\theta)$ is the antenna array gain pattern in the azimuth direction. For analytical simplicity, the gain is assumed to be constant so that $G(\theta) = M$ where M denotes the number of the antenna array elements.

Substituting the pdf in (11) in (13), the DPS of the diffused component of the wavefield is plotted in Fig. 3 for $\sigma_m = 30$ m, $\sigma_m = 60$ m and $\beta = 60^\circ$.

$$S_d(f) = \frac{p}{\sqrt{f_m^2 - f^2}} \left[G(\theta) \cdot p_d \left(\phi_v + \left| \cos^{-1} \left(\frac{f}{f_m} \right) \right| \right) + G(-\theta) \cdot p_d \left(\phi_v - \left| \cos^{-1} \left(\frac{f}{f_m} \right) \right| \right) \right] \quad (13)$$

$$a(\tau) = J_0(2\pi f_m \tau) \int_{-\beta}^{\beta} p_d(\theta) d\theta + 2 \cdot \sum_{v=1}^{\infty} (-1)^k \cdot J_{2k}(2\pi f_m \tau) \cdot \int_{-\beta}^{\beta} \cos(2k(\phi_v - \theta)) p_d(\theta) d\theta + \sqrt{1 - m^{-1}} \cdot \cos(2\pi f_m \tau \cos \theta_{LOS}) \quad (14)$$

$$c(\tau) = 2 \cdot \sum_{k=0}^{\infty} (-1)^k J_{2k+1}(2\pi f_m \tau) \cdot \int_{-\beta}^{\beta} \cos[(2k+1)(\phi_v - \theta)] \cdot p_d(\theta) d\theta + \sqrt{1 - m^{-1}} \cdot \sin(2\pi f_m \tau \cos \theta_{LOS}) \quad (15)$$

This plot shows that: (i) The direction of motion has a modulating effect on the Doppler power spectra. When the MS moves perpendicularly to the direct path (BS-MS base line), $\phi_v = 90^\circ$, the spectral contents concentrate near the 0 Hz as shown in Fig. 3. (ii) The effect of the MS scatterer's variance on the DPS, where increasing the variance has a broadening effect on the Doppler power spectrum. The temporal correlations of the total wavefield, using results in [Stüber, 2001] and trigonometric expansions of Bessel functions in [Gradshteyn and Ryzhik, 1980] can be expressed as given in (14) and (15). The plots of $a(\tau)$ (the auto-correlation function) and $c(\tau)$ (the cross-correlation function) for different values of received angular

spread and $\beta=60^0$ are shown in Fig. 4, 5 and 6. These plots show two important results: (i) The temporal auto-correlations and cross-correlations have a damped oscillations pattern. The damping rate increases as the angular spread increases. Hence, the damping rate of the auto-correlation function of a wave-field that has a small angular spread is much slower than the damping rate of the zeroth-order Bessel function (Clarke’s model) where the received wave-field is distributed over the angular range $[0, 2\pi]$. (ii) The cross-correlation function is non-zero which implies that the assumption of having un-correlated and hence independent in-phase and quadrature Gaussian processes, leading to the Rayleigh envelope statistics, is valid only when the AoA pdf is uniform over the range $[0, 2\pi]$ for all the values of τ (at any observation time) or at the observation instants which corresponds to the zero crossings of the cross-correlation function for other AoA distributions.

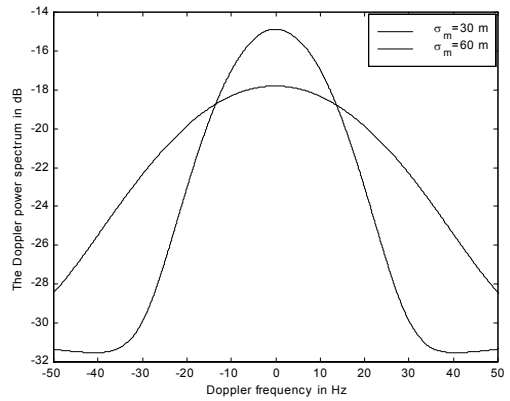
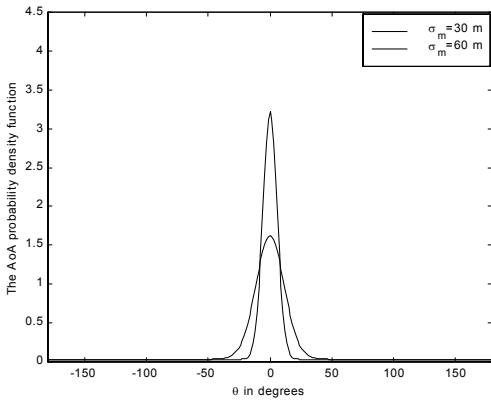


Figure 2: The AoA pdf of the diffused wavefield for different values of the MS scatterer’s variance.

Figure 3: The DPS of the diffused wavefield for different values the MS scatterer’s variance.

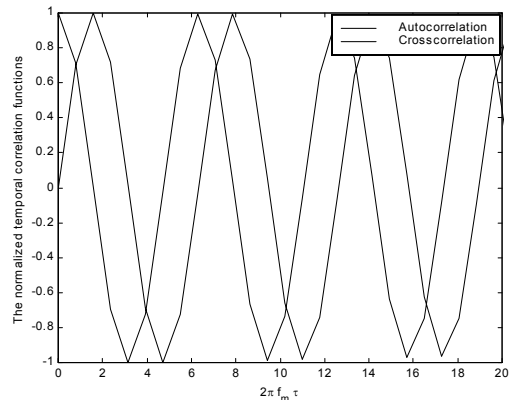
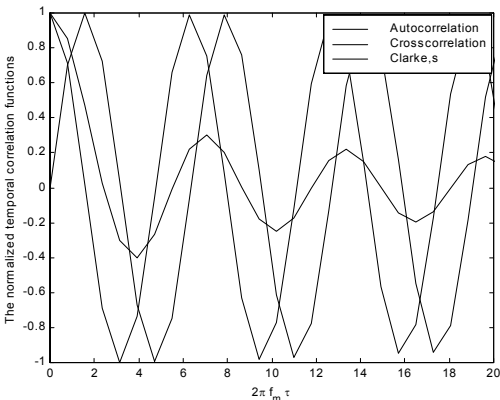


Figure 4: The temporal correlations of the received wavefield for $\sigma_m=40$ m and $D= 300$ m.

Figure 5: The temporal correlations of the received wavefield for $\sigma_m=40$ m and $D= 500$ m.

3.4. Spatial Correlations

One of the main concerns in the analysis of the performance of antenna arrays systems in multi-path fading channels is the spatial correlation between the signals received at the i th and the k th antenna elements. The spatial correlation is defined as a measure of the correlation between the amplitudes of multi-path components that arrive with the same excess delay at the ULA (uniform linear array). Using the geometrical model of an ULA, with element spacing (d) and mean of direction of arrival (ϕ_0), the normalized spatial power correlation coefficient between a multi-path component received at the element “ k ” and its replica at the element “ l ” can be expressed as [Salz and Winters, 1994].

$$R = \left(|R_{xx}|^2 + |R_{yy}|^2 \right)^{1/2} \tag{16}$$

where R_{sxx} and R_{sxy} denote the spatial correlations among real and imaginary components of the faded signals (at elements k and l). Assuming that the reference wave-front plane coincides with the reference element (k) (usually the center element), then, the wave arriving at the adjacent element (l) suffers a phase delay (τ) relative to the element (k) that is given as

$$\tau = \frac{2\pi d}{\lambda} \sin \phi \quad |\phi| \leq \pi \tag{17}$$

and $(M - k) \cdot \tau$ at element “ M ”

using a similar procedure to the one given in [Salz and Winters, 1994], R_{sxx} and R_{sxy} can be derived as given in (18) and (19). The integrals in (18) and (19), can not be analytically solved, so numerical integration is used to compute these integrals. The results are shown in Fig. 7, 8 and 9 for different values of the mean angles of arrival (ϕ_0), the MS- BS distance (D) and the fading parameter m .

$$R_{xx}(k-l) = \int_{\phi_0-\beta}^{\phi_0+\beta} J_0(z(k-l)) p_d(\theta) d\theta + 2 \cdot \sum_{v=1}^{\infty} J_{2k}(z(k-l)) \cdot \int_{\phi_0-\beta}^{\phi_0+\beta} \cos(2k(\phi_v - \theta)) p_d(\theta) d\theta + \sqrt{1-m^{-1}} \cdot \cos(z \sin(\phi_v - \theta_{LOS})) \tag{18}$$

$$R_{xy}(k-l) = 2 \cdot \sum_{k=0}^{\infty} J_{2k+1}(z(k-l)) \cdot \int_{\phi_0-\beta}^{\phi_0+\beta} \sin[(2k+1)(\phi_v - \theta)] p_d(\theta) d\theta + \sqrt{1-m^{-1}} \cdot \sin(z \sin(\phi_v - \theta_{LOS})) \tag{19}$$

where $z = \frac{2\pi d}{\lambda}$. From these results, the following observations can be stated: (i) The spatial correlations increase as the mean AoA increases (as measured from the broadside line). This can be seen in Fig. 7 where the minimum correlation coefficient is at $\phi_0 = 0^0$. Such a result has been reported in previous research for other AoA distributions (uniform [Salz and Winters,

1994], raised-cosine [Lee, 1973], and truncated gaussian [Adachi et al, 1986]). (ii) The spatial correlation coefficient increases as the illuminated physical angular spread (by the ULA main beam) increases. Hence, for a certain beam-width, as the parameter σ_m increases or the parameter D decreases, the spatial angular spread increases, which reduces the spatial correlations. This is shown in Fig. 8 where decreasing D from 500m to 300m reduces the spatial correlation coefficient (for a Rayleigh faded signal) from 0.45 for $D=500$ m to 0.12 for $D=300$ m for $d=5\lambda/2$. (iii) Multi-path components (Nakagami faded with $m>1$) are highly correlated due to the existence of the LOS component. This correlation increases up as the amplitude of the LOS component increases to the non-fading case ($m= \infty$) where the envelope correlation coefficient becomes unity. This is shown in Fig. 9 for ($m=2$) as compared to $m=1$ where the correlation coefficient for $m=2$ remains high (>0.75) irrespective of the increase in the inter-element spacing.

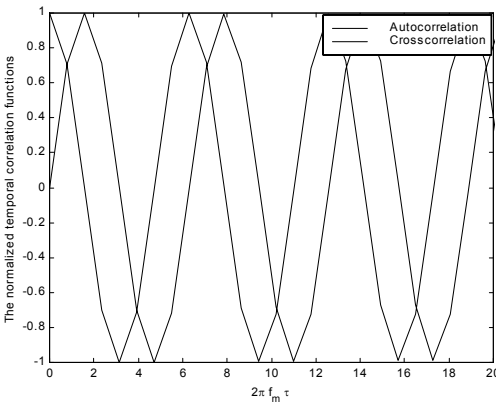


Figure 6: The temporal correlations of the wavefield for $m=2$, $\sigma_m=40$ m and $D= 500$ m.

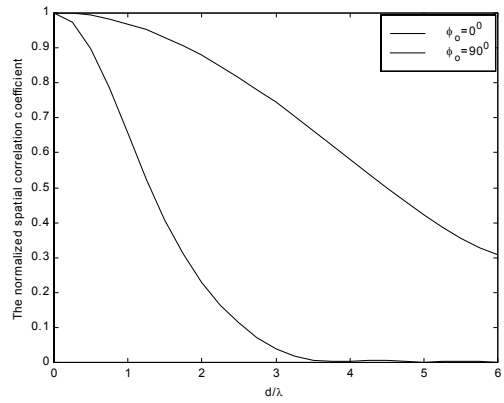


Figure 7: The spatial correlation coefficient of a Rayleigh faded path for $\phi_o= 0^0$ and $\phi_o=90^0$.

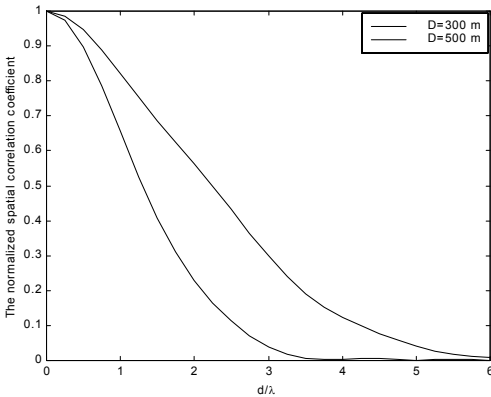


Figure 8: The spatial correlation coefficient of a Rayleigh faded path for $D=300$ m and $D=500$ m.

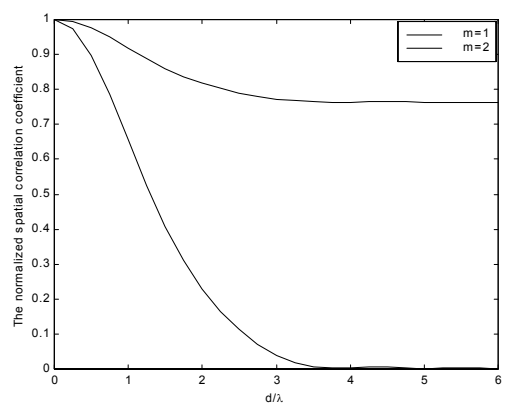


Figure 9: The spatial correlation coefficients of Nakagami faded paths with $m=1$ and $m=2$.

4. BU (BAD URBAN) CHANNELS

4.1. Channel Geometry and Scatterers Distributions

A bad urban environment is characterized by the existence of a mixture of open areas and densely built-up zones with a large variety of different building heights. The equivalent model of the scattering and propagation mechanisms in a bad urban environment has the same geometry of the wideband elliptical model, see Fig. 10.

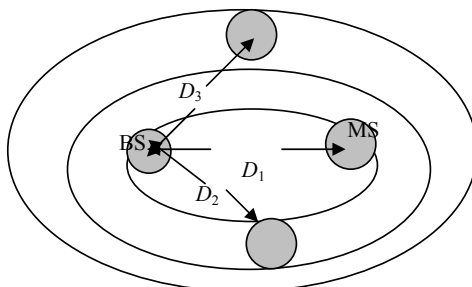


Figure 10: The geometrical model of BU channels.

Each path is assumed to be due to a cluster of scatterers, which lie in between the concentric ellipses with foci at the BS and the MS, respectively. The scatterers around the MS (with a radius R_1) generate the first arriving multi-path component at the BS receiver; the second cluster of scatterers (within the second ellipse and with a radius R_2) should generate the second path and so on for the other paths. In the context here, a three-path model is considered. Clearly, this model can be extended to any number of paths. Since most of the effective scatterers around the BS lie in the area of the ellipse that corresponds to the first path, only the contribution of the BS scatterers to the first path is considered. The joint density of the BS clusters scatterers being illuminated by the first beam is the same pdf as given in (7). So that

$$p_b(r_b, \theta) = \frac{1}{2\pi\sqrt{2\pi}\sigma_b} \exp \left[-\frac{\left(r_b - \frac{R_{b1}}{2}\right)^2}{2\sigma_b^2} \right] \tag{20}$$

The scatterer's pdf's, assuming that the scatterers (in the three clusters) have the (bi-variate Gaussian) distribution, can be expressed, using (5) as,

$$p(r_b, \theta) = \frac{r_b}{2\pi\sigma_i^2} \cdot \exp \left[-\frac{r_b^2 - 2r_b D_i \cos \theta + D_i^2}{2\sigma_i^2} \right], \quad i = 1, 2, 3. \tag{21}$$

where D_2 and D_3 denote the distances between the BS and the centers of the clusters as shown in Fig. 10. The distances D_2 and D_3 can be calculated for the set of the mean AoA's (ϕ_2 and ϕ_3) using the equations of the ellipses that correspond to the average delay of each path as [Janaswamy, 2001]

$$D_2 = \frac{4a_2^2 - D^2}{4a_2 - 2D \cos \phi_2} \tag{22}$$

$$D_3 = \frac{4a_3^2 - D^2}{4a_3 - 2D \cos \phi_3} \tag{23}$$

where a_2 and a_3 are given as

$$a_2 = \frac{D}{2} + R_1 + R_2 \tag{24}$$

$$a_3 = \frac{D}{2} + R_1 + 2R_2 + R_3 \tag{25}$$

4.2. AoA Statistics

The AoA pdf of each of the multi-path components can be determined using (8) for the first path (which may contain the LOS component) and the following modified pdf for the other paths

$$p(\theta) = (1 - \sqrt{1 - m^{-1}}) \cdot p_d(\theta) + \sqrt{1 - m^{-1}} \cdot \delta(\theta - \theta_{SPC}) \tag{26}$$

where θ_{SPC} denotes the AoA of the specular component contained in that path¹.

The pdf of the diffused component $p_d(\theta)$ is given in (9). However, the AoA's pdf due the BS and the MS scatterers have to be derived according to new geometrical model given in Fig. 10.

To derive the pdf's of the diffused components of each path, the approach in the previous part can be used. The pdf of the TIS's of the first path, due to the BS scatterers, can be derived using the pdf in (20) as

$$p(\theta) = \frac{1}{4\pi} \cdot \left[erf\left(\frac{R_{b1}}{2\sqrt{2}\sigma_b}\right) + erf\left(\frac{R_{ns1} - \frac{R_{b1}}{2}}{\sqrt{2}\sigma_b}\right) \right] \tag{27}$$

¹ - A specular component is distinguished from a Line-of-Sight component by the arrival of the signal because of scattering process. Hence, a LOS component is associated with the first path and specular components can be associated to any other path due to the existence strong reflectors.

where R_{b1} and R_{ns1} are analogous to R_b and R_{ns} in the third part in (11). The AoA pdf of the TIS's of the three paths (due to the three clusters) can be derived by substituting the scatterer's pdf's in (21) in (10), with the appropriate parameters. Carrying out integration gives the AoA pdf's for diffused components of the first, second and third paths, are given in (28).

$$\begin{aligned}
 p(\theta) = & \frac{1}{2\sqrt{2\pi}\sigma_i} \cdot D_i \cos\theta \cdot \exp\left[\frac{D_i^2(\cos^2\theta - 1)}{2\sigma_i^2}\right] \cdot \left[\operatorname{erf}\left(\frac{bb_i - D_i \cos\theta}{\sqrt{2}\sigma_i}\right) + \operatorname{erf}\left(\frac{aa_i - D_i \cos\theta}{\sqrt{2}\sigma_i}\right) \right] \\
 & + \left(\frac{1}{2\pi}\right) \cdot \exp\left(\frac{-D_i^2}{2\sigma_i^2}\right) \cdot \left\{ \exp\left[\frac{-aa_i(aa_i - 2D_i \cos\theta)}{2\sigma_i^2}\right] - \exp\left[\frac{-bb_i(bb_i - 2D_i \cos\theta)}{2\sigma_i^2}\right] \right\}, |\theta| \leq \beta_i \\
 & , i = 1, 2, 3.
 \end{aligned}
 \tag{28}$$

The parameters in (28), are given as

$$aa_i(\theta) = D_i \cos\theta - \sqrt{D_i^2 \cos^2\theta - D_i^2 + R_i^2}
 \tag{29}$$

$$bb_i(\theta) = D_i \cos\theta + \sqrt{D_i^2 \cos^2\theta - D_i^2 + R_i^2}
 \tag{30}$$

and

$$\beta_i = \sin^{-1}\left(\frac{R_i}{D_i}\right) , i = 1, 2, 3.
 \tag{31}$$

The values parameters R_1 , R_2 , and R_3 can be determined from the geometry in Fig. 10. The values of the radii are determined by the resolution of the W-CDMA channel ($t \approx 1/W$). For example, in a 3.844 MHz channel, the resulting resolution is .26 ms. So, if the first path arrives at an average delay of t_0 , then the second path will arrive at an average delay of $t_0 + .26$ ms which corresponds to a path length difference of 78 m. So, the difference between the second and third ellipses will be 78 m and hence the radii of the circles. The plots of the three paths AoA's pdf's are shown in Fig. 11. Clearly, BU environments do generate multi-paths in both the spatial and temporal domains. Wide-band impulse response measurements in such environments in [Pederson et al, 2000], [Braun and Dersch, 1991] and [Suzuki, 1979] have recorded the occurrence of strong peaks in the impulse responses, which are due to the separate clusters of scatterers [Braun and Dersch, 1991]. So, the equivalent channel impulse response is given by (1) where the number of the spatio-temporally distinct effective clusters determines the parameter L .

4.3. Doppler Power Spectrum and Temporal Correlations

The Doppler power spectrum of the first multi-path component in the BU model can be derived using (12) where the AoA pdf's (of the diffused components), are given in (27) and

(28), respectively. The Doppler power spectra of the received diffused wave-field corresponding to the second and the third paths are given by substituting the AoA pdf's into the expression in (13). However, for the second and third paths, the virtual angles of the MS velocity relative to the one of the first path have to be considered. So, if the MS is moving towards the BS ($\phi_1=0$) then the virtual angle of velocity of the second path (ϕ_{v2}) will equal to the angle of shift of this path relative to the BS-MS baseline and similarly for the third path. Hence, in the model considered here, since the second and the third paths have mean AoA's of 30° and 40° , then the virtual angles of MS velocity are given as $\phi_{v2}=30^\circ$ and $\phi_{v3}=-40^\circ$. The plot of the Doppler power spectra is shown in Fig. 12 for the first, second and the third paths respectively. This plot shows that the spectral contents of the paths are concentrated in a narrow frequency range as a direct consequence of the small angular spread of the paths. Also, these plots show the difference between the Doppler spectra of the second and third paths from the first path Spectra due to the effect of the virtual angles of the MS velocity. For example, for $\phi_v = 90^\circ$ while the Doppler Spectrum of the first path is centered at 0 Hz corresponding to $(f_m \cos(\phi_v)=100 \cos(90^\circ)=0$ Hz), the spectrum of the second path is centered at (-50Hz) which corresponds to $(f_m \cos(\phi_{v2})=100 \cos(90+30)=-50$ Hz) and similarly the third path (see Fig. 12). The temporal auto-correlation and cross-correlation functions of the three multi-path components can be computed by substituting the AoA pdf of each path into the expressions of the temporal correlations. So, substituting the pdf's in (27) and (28) into (14) and (15), and taking into consideration the concept of the virtual angles of the MS velocity as discussed in the Doppler power spectra part, the autocorrelation and cross-correlations can be computed using numerical integration schemes. The results are shown in Fig. 13 and 14 for the first and second paths, respectively. Those plots show that the two paths have sinusoidal correlation functions with very small decaying rates. The decaying rates increase virtual angle of motion increases, which can be observed by comparing the correlation functions of the first and second paths.

4.4. Spatial Correlations

The spatial correlations of the three paths can be computed using procedure used for the BU single path. The plots of the envelope spatial correlation coefficients the signals corresponding to the first path, the second path and third paths are shown in Fig. 15 for different values of the standard deviation of the clustered scatterers. The results show that the paths are highly correlated relative to the TU model due the smaller spread (variance) of scatterers ($\sigma_1=30$ m, $\sigma_2=20$ m and $\sigma_3=15$ m). The effect of the BS scatterers on the spatial correlations is shown in Fig. 16 where the contribution of the BS scatterers decreases the spatial correlation coefficient at the BS receiver. Such a result was reported by field measurement [6], however, the decrease is small due to the smaller probability of the contribution of the BS scatterers in the scattering process relative to the MS scatterers.

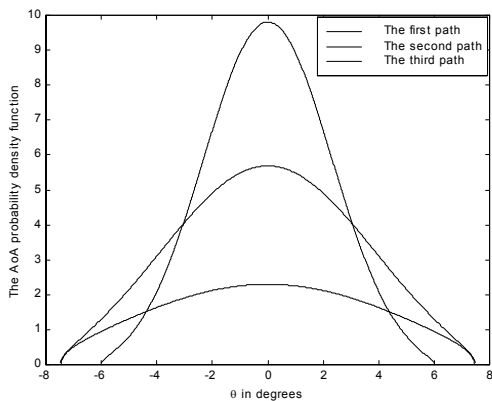


Figure 11: The AoA pdf 's of the first, second and third paths for $\sigma_1=30$ m, $\sigma_2=20$ m and $\sigma_3=15$ m.

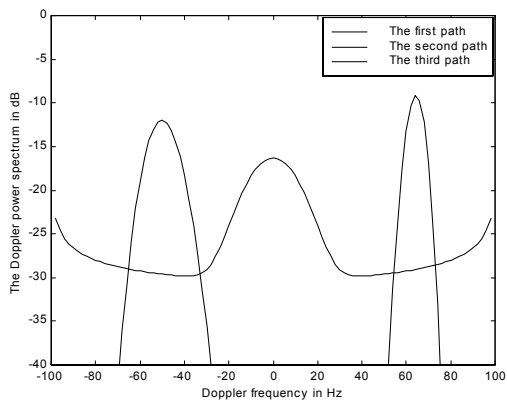


Figure 12: The Doppler spectra of the first, second and third paths for $\sigma_1=30$ m, $\sigma_2=20$ m and $\sigma_3=15$ m.

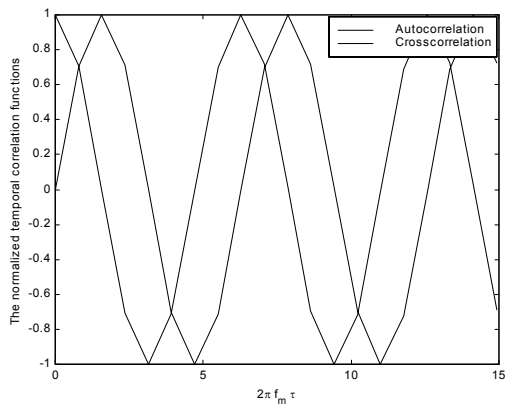


Figure 13: The temporal correlations of the first path for $m_1=1$ and $\sigma_1=30$ m.

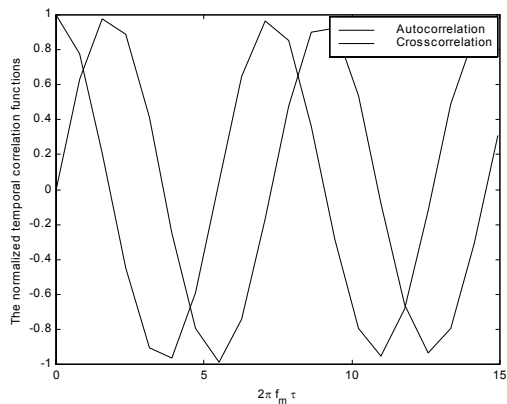


Figure 14: The temporal correlations of the second path for $m_2=1$ and $\sigma_2=20$ m.

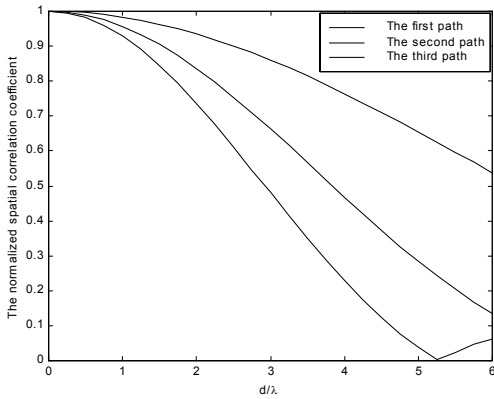


Figure 15: The spatial correlation coefficients for the three paths with $\sigma_1=30$ m, $\sigma_2=20$ m and $\sigma_3=15$ m.

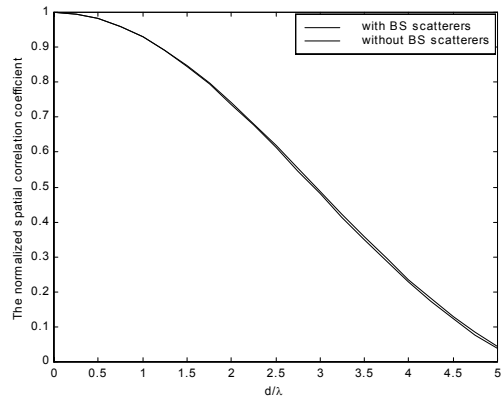


Figure 16: The spatial correlation coefficient of the first path for the cases: with the BS scatterers effect and without it.

5. CONCLUSIONS

In this paper, geometrically-based modeling was utilized to spatially characterize both wideband TU and BU Nakagami faded channels. The appropriate geometrical models (wideband elliptical models and scatterer's distributions (bi-variate Gaussian distributions) were used to derive the AoA statistics. Then, the temporal and spatial correlations were computed for different channel conditions (scatterer, s variance, BS-MS distance, MS direction of motion, mean AoA and the fading parameter m). The obtained results have shown the following important results:

Bad urban environments are expected to generate spatio-temporal responses with temporal and spatial distinct paths (each path has a distinct average delay and a distinct mean AoA). On the other hand, typical urban environments are expected to have spatio-temporal impulse responses with strong early peak (path) followed by temporally (possibly) distinct paths with no spatial selectivity.

The AoA statistics of each of the received multipath components (at the BS receiver) are not uniform. The AoA distributions can be approximated by truncated Gaussian or truncated Laplacian distributions, which do agree with the results of measurements, conducted in both TU and BU environments.

The temporal correlation functions have complex damping sinusoidal patterns. The damping rate decreases as the received angular spread decreases due to the small variance of the cluster scatterers or the use of highly directive beams. This can be seen in BU environments when

spatially selective (2-D RAKE) receivers are used the BS leading to periodic (cyclostationary) correlation functions for a quite significant range of τ .

The spatial correlations in both TU and BU environments decrease as the illuminated angular spread (by the BS receiver) increases and the existence of the LOS component leads to high spatial correlation coefficients.

The presence of the local scatterers at the BS reduces the spatial correlations at the BS receiver especially in BU environment where the contribution of the BS scatterers is expected to be more significant. Also, it was found that the direction of MS motion (relative to the LOS) effects the pattern of the spatial correlations which was not analytically previously investigated.

REFERENCES

Adachi, F., M. Feeney, A. Williamson, and J. Parsons, "Crosscorrelation between the envelopes of 900 MHz signals received at a mobile radio base station site," *IEE Proc. Pt. F.*, vol. 133, no. 6, pp. 506-512, October 1986.

Braun, W.R. and U. Dersch. A Physical Mobile Radio Channel Model. *IEEE. Trans. Veh. Technol.*, vol. 40. NO, 2, MAY. 1991.

Chia, S.T., R. Steele, E. Green and A. Baran, "Propagation and bit error rate measurements for a micro-cellular system," *J. IERE*, 57(6), S255- 66 (suppl). 1987.

Fuhl, J., A.F. Molisch, and E. Bonek, " Unified channel model for mobile radio systems with smart antennas," *IEE Proc.- Radar, Sonar, Navig.*, vol. 45, pp. 32-41, 1998.

Gradshteyn, I.S. and I. M. Ryzhik, *Table of Integrals, Series, and Products*. New York: Academic, 1980.

Jakes, W.C., *Microwave mobile communications*. John Wiley, NY, 1974.

Janaswamy, K., *Radio-wave propagation and smart antennas for wireless communications*. Kluwer Academic Publishers. Massachusetts. 2001.

Lee, W.Y.C., "Effects on correlation between two mobile radio base-station antennas," *IEEE Trans. on Commun.*, vol. 21, no. 11, pp. 1214- 1224, November 1973.

Papoulis, A., *Probability Random Variables and Stochastic Processes*. New York, NY: McGraw- Hill, 1984.

Pederson, K.I., P. E. Mogensen, and B. H. Fleury, "A stochastic model of the temporal and azimuthal dispersion seen at the base station in outdoor propagation environments," *IEEE Trans. Veh. Technol.*, vol. 49, no. 2, March. 2000.

Salz, J. and J. H. Winters, "Effect of fading correlation on adaptive arrays in digital mobile radio," *IEEE Trans. Veh. Technol.* Vol. 43, no. 4, pp. 1049-1057, Nov. 1994.

Stüber, G.L., *Principles of mobile communications*. Kluwer Academic Publishers. MA, 2001.

Suzuki, H., "A Statistical Model for Urban Radio Propagation," *IEEE. Trans. on Comm*, vol. COM-25, pages 973-980, July. 1979.

Turkmani, A.M.D., J. D. Parsons, F. Ju and D. Lewis, " Micro-cellular radio measurements at 900, 1500 and 1800 MHz," *Proc. 5th Int. Conf. On Land Mobile Radio*, Warwick, pp. 65-68. 1989.